Available online at www.sciencedirect.com
SCIENCE DIRECT
Journal of Catalysis 241 (2006) 312–318
JOURNAL OF CATALYSIS
www.elsevier.com/locate/jcat

Discovery of a new catalytically active and selective zeolite (ITQ-30) by high-throughput synthesis techniques

Avelino Corma *, Mª José Díaz-Cabanas, Manuel Moliner, Cristina Martínez

Instituto de Tecnología Química, UPV-CSIC, Universidad Politécnica de Valencia, Avda. de los Naranjos s/n, 46022 Valencia, Spain

Received 20 January 2006; revised 5 April 2006; accepted 6 April 2006

Available online 9 June 2006

Abstract

By applying a sequential design of experiments, high-throughput syntheses, and X-ray diffraction and data-mining techniques, it has been possible to synthesize a new zeolite (ITQ-30) within a wide range of Si/Al ratios (10–∞). Structurally, ITQ-30 belongs to the MWW family, with disordered layers as MCM-56. Its large external surface area makes this zeolite an active and selective catalyst for alkylation of benzene with propylene.

Keywords: ITQ-30; HT zeolite synthesis; MWW zeolite family; Benzene alkylation to cumene with ITQ-30

1. Introduction

Synthesis of zeolites involves the interplay of numerous variables [1]. Traditional synthesis methods in which one variable at a time is modified usually require a long time to explore a large volume of the synthesis phase diagram. The application of high-throughput (HT) techniques to zeolite synthesis reduces the screening time and increases the number of experiments that can be conducted for each system without impeding researchers to think [2–4]. Thus more synthesis variables can be studied at a higher level, increasing the probability of finding new materials while achieving better understanding of the crystallization mechanisms.

A general HT strategy applied to zeolite synthesis can be summarized as follows [5]. First, based on previous knowledge, the synthesis variables to be studied are defined and a factorial design is selected to cover the compositional zone to be investigated. Then, all samples are automatically synthesized by means of robotic systems and characterized by HT X-ray diffraction (XRD). However, it should be taken into account that HT synthesis and characterization generates a high number of results, which require the application of data-mining techniques [6] to extract all possible information.

In our case, because several large- and ultralarge-pore zeolites (e.g., SSZ-24 [7], CIT-5 [8], and ITQ-21 [9]) have been synthesized using *N*-methyl-sparteinium (MSPT) as an organic structure-directing agent (SDA) (Fig. 1), we investigated whether this large and rigid cation could produce new structures. By expanding the region of the phase diagram studied by means of HT synthesis, the possibility of obtaining new large- or ultralarge-pore zeolites has been explored. We report a new large-pore zeolite, ITQ-30, which exhibits interesting catalytic properties, obtained by applying this methodology. Furthermore, we show how the application of data-mining techniques enables extraction of fundamental information that can be used to discuss zeolite synthesis mechanism.

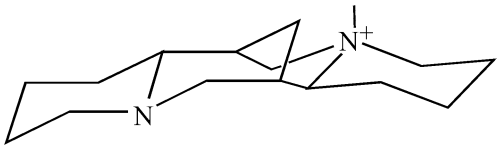

Fig. 1. Structure directing agent used in this work: *N*(16)-methyl-sparteinium.

* Corresponding author. Fax: +34 96 3877809.
E-mail address: acorma@itq.upv.es (A. Corma).

0021-9517/$ – see front matter
doi:10.1016/j.jcat.2006.04.036

2. Experimental

2.1. Materials

The gel composition was evaluated by varying the molar ratios of Al/(Si + Ge), MSPT/(Si + Ge), F^-/(Si + Ge), and Si/Ge, producing samples with the general formula

$$x\mathrm{GeO_2}:(1-x)\mathrm{SiO_2}:y\mathrm{Al_2O_3}:z\mathrm{MSPTOH}:z\mathrm{NH_4F}:w\mathrm{H_2O}.$$

Synthesis gels were prepared using an in-house-developed robotic system composed of (i) robotic arm (SCORBOT-ER 4pc), for vial handling and solids weighing (range, 20–1000 mg); (ii) stirring station, for gel stirring and solvent evaporation by IR heating and Air/N_2 sweep flow; and (iii) liquid dosing station equipped with seven calibrated syringe pumps (range, 10–5000 mg) and an analytical balance. Automated gel synthesis was carried out inside 3-mL Teflon vials, allowing the preparation of 15 samples.

In a typical synthesis, a solution of *N*(16)-methyl-sparteinium hydroxide [7], Ludox AS-40 (colloidal silica, 40 wt% suspension in water, Aldrich), germanium oxide (99.998%, Aldrich), and aluminum isopropoxide (98+%, Aldrich) was added by the robot arm, and the mixture was stirred until homogenization occurred. Then the ammonium fluoride (98+%, Aldrich) was added, and the mixture was stirred until the desired composition was reached. Finally, the Teflon vials were inserted in a multiautoclave with 15 positions formed by Teflon-lined hollows made in a steel block and covered first with Teflon, then with steel, and heated to 175 °C. The solids were then filtered and washed in parallel and dried at 100 °C overnight. Synthesized samples were characterized by powder XRD using a multisample Philips X'Pert diffractometer using CuK_α radiation. Scanning electron microscopy (SEM) images were obtained using a JEOL JSM-6300 microscope.

2.2. HT and data-mining techniques

A factorial experimental design ($4 \times 3^2 \times 2^2 = 144$) was selected to study crystallization time and gel composition simultaneously, varying the molar ratios of the components Al/(Si + Ge), MSPT/(Si + Ge), F^-/(Si + Ge), and Si/Ge. Table 1 gives the values and levels considered for the different variables.

Pareto analysis is a statistical method that allows quantification of the hypothetical weight of each variable in the final result. The resulting chart is a frequency histogram that arranges the parameters according to their influence, with the most important on top. In this chart, the length of each bar is the estimated effect divided by its standard error, which is equivalent to computing a *t*-statistic for each effect. Bars extending beyond the vertical line on the plot correspond to effects that are statistically significant at a 95% confidence level. This statistical approach to interpreting the results allows quantification of the hypothetical weight of the factors in the growth of materials.

Table 1
Synthesis conditions in the first set of experiments: values and levels considered for the different variables

	Nr. level	Variation ranges			
		Level 1	Level 2	Level 3	Level 4
Time (days)	2	1	5		
Si/Ge	4	15	20	25	50
Al/(Si + Ge)	3	0.02	0.04	0.067	
MSPT/(Si + Ge)	2	0.25	0.5		
F/(Si + Ge)	2	0.25	0.5		
H_2O/(Si + Ge)	3	2	5	10	

2.3. Catalytic experiments

Alkylation of benzene with propylene was carried out with the zeolites in acid form that were pelletized, crushed, and sieved at 0.25–0.42 mm diameter. These acid samples were obtained directly by calcination at 540 °C in air for ITQ-30 and MCM-22 and after ion exchange (0.25 M NH_4Cl solution, 80 °C, liquid/solid ratio = 10, 1 h) and in situ calcination at 520 °C for MCM-56. The reaction was performed in an automated high-pressure stainless steel reactor at 150 °C, 3.5 MPa, a benzene/propylene molar ratio = 3.5, and a WHSV = 6 h^{-1}. Under these conditions, the reaction occurred in the liquid phase. Samples were analyzed by gas chromatography at various times by means of a 30-m 5% phenyl–95% dimethylpolysiloxane column with an internal diameter of 0.25 mm and a phase film thickness of 1 μm. The ITQ-30 samples were also characterized by Ar and N_2 adsorption isotherms, measured with a Micromeritics ASAP 2000 instrument.

3. Results and discussion

Two zeolites were found in the area of the phase diagram studied: ITQ-21 and a new material designated as ITQ-30. The XRD patterns of both materials are shown in Fig. 2. Automatic calculation of the occurrence and crystallinity of the phases was done by integrating the area of the characteristic peaks for each phase and referring this to the fully crystalline materials. For ITQ-30, the 2θ angle range is at 24.6°–25.4°; for ITQ-21, the integrated area is at 25.4°–27.2°. Because ITQ-30 also presents diffraction peaks in the 25.4°–27.2° region, the percentage of ITQ-30 is subtracted considering the crystallinity measured from the peak located at 25.0°.

Fig. 3 presents a phase diagram obtained following the factorial design described above and the areas in which ITQ-21, ITQ-30, or amorphous material predominates. A first approach using Pareto analysis (Fig. 4) reveals the relative influence of each synthesis variable on the crystallinity of ITQ-21 and ITQ-30. Both ITQ-21 and ITQ-30 zeolites seem to be negatively influenced by water and aluminum content; that is, the more dilute the gels or the higher the Al/(Si + Ge) ratios, the less crystalline the samples. Furthermore, high MSPT/(Si + Ge) and F/(Si + Ge) ratios play positive roles in the formation of ITQ-21 and ITQ-30.

Some important differences can be observed when comparing ITQ-21 and ITQ-30, however. On one hand, the relative importance of MSPT/(Si + Ge) and F/(Si + Ge) is greater for ITQ-30, because this material is obtained in only a few cases with the lowest content of MSPT/(Si + Ge) and F/(Si + Ge).

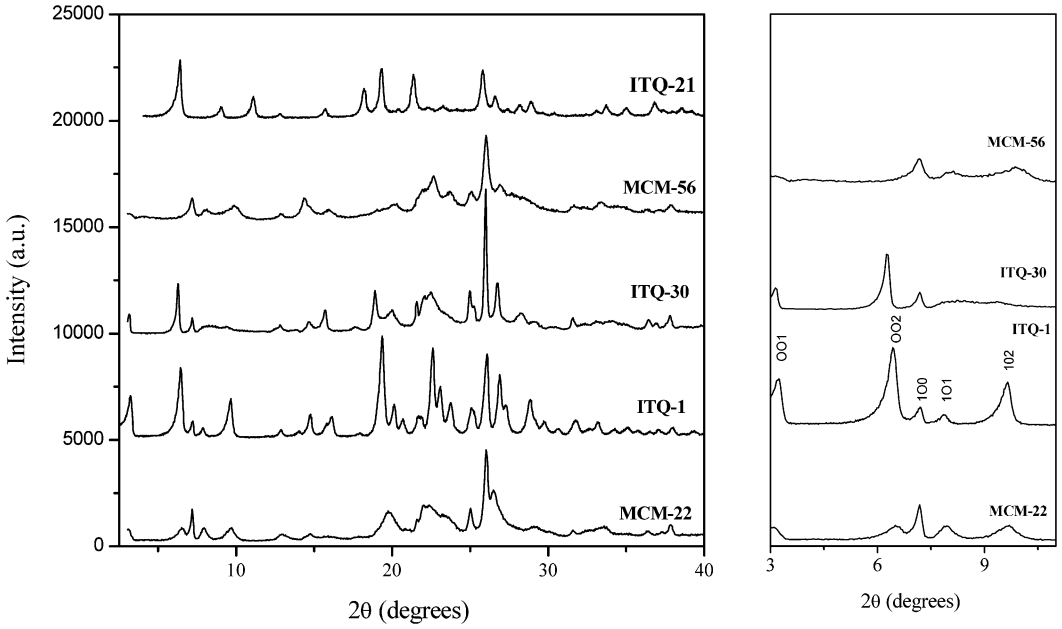

Fig. 2. X-ray diffraction patterns of different zeolites of the MWW family, ITQ-30 and ITQ-21.

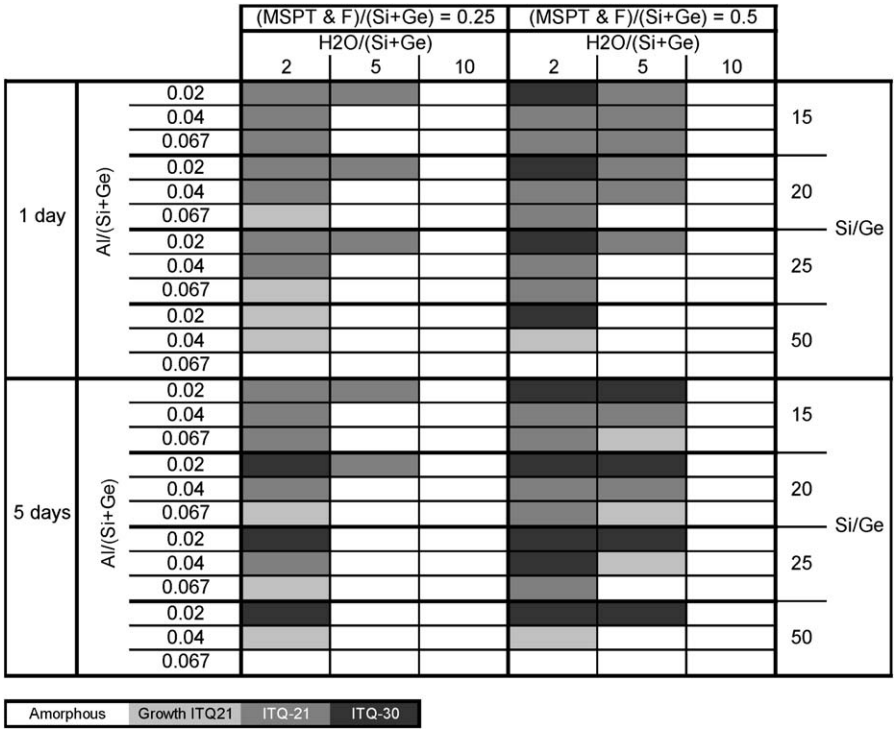

Fig. 3. Experimental regions for appearance of amorphous, ITQ-21 and ITQ-30 materials.

On the other hand, a higher Si/Ge ratio appears to be an important negative factor in ITQ-21 crystallization, whereas it is a slightly positive factor in ITQ-30 synthesis. This result must be considered a drawback for the growth of ITQ-21 when increasing the Si/Ge ratio, because in that case ITQ-30 will be favoured. Thus, the Si/Ge ratio variable can be a favourable factor in obtaining pure ITQ-30 zeolite. Finally, the relative influence of the crystallization time for these materials indicates that ITQ-21 will be a primary product transformed into ITQ-30 at longer crystallization times, demonstrating the greater thermodynamic stability of the ITQ-30 structure. In summary, our initial factorial synthesis design and data-mining techniques have revealed a new zeolitic structure, ITQ-30, that can compete with ITQ-21, and the possibility exists that pure ITQ-30 can be obtained through further work on the crystallization time and the Si/Ge ratio of the gel.

Several new zeolites [9–13] have been obtained by adding germanium to the synthesis gels [14]. However, for industrial

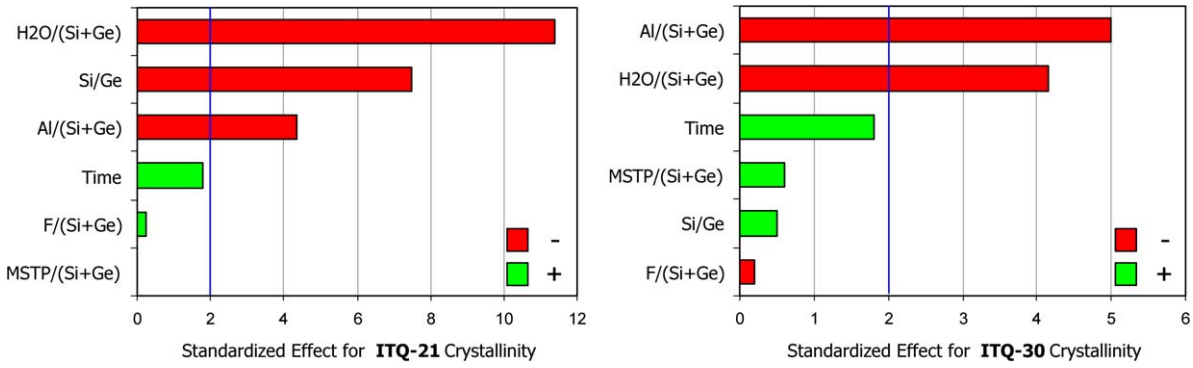

Fig. 4. Pareto analysis showing the relative influence of each synthesis variable over crystallinity of the different phases.

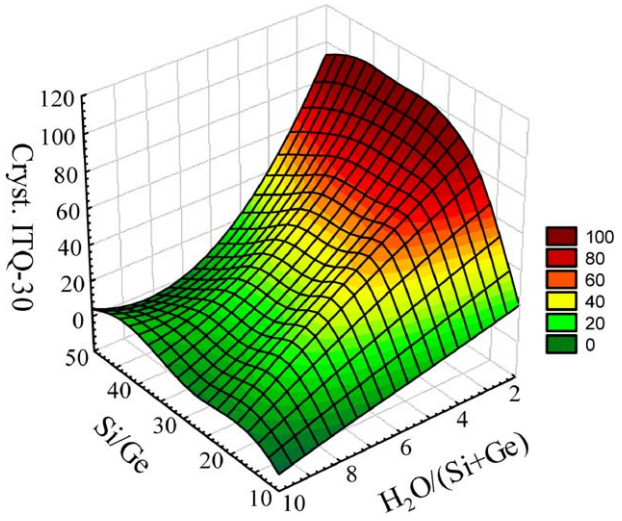

Fig. 5. Three-dimensional chart showing the evolution of ITQ-30 crystallinity. Synthesis conditions: 5 days; Al/(Si + Ge) = 0.02; MSPTF/(Si + Ge) = 0.5.

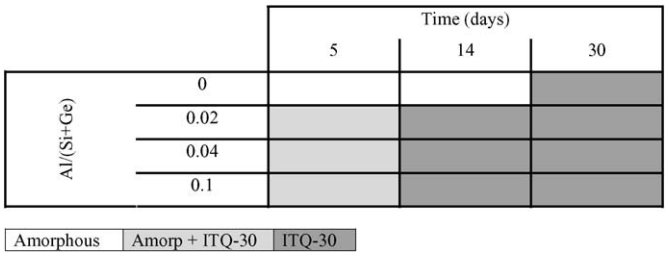

Fig. 6. Synthesis of ITQ-30 for different crystallization times and Ge contents.

Table 2
Synthesis conditions in the second set of experiments: values and levels considered for the different variables

	Nr. level	Variation ranges			
		Level 1	Level 2	Level 3	Level 4
Time (days)	3	5	14	30	
Si/Ge	1	∞			
Al/(Si + Ge)	4	0	0.02	0.04	0.1
MSPT/(Si + Ge)	1	0.5			
F/(Si + Ge)	1	0.5			
H_2O/(Si + Ge)	1	2			

Table 3
Chemical analysis of different ITQ-30 samples synthesized in the Si/Al ratio from 10 to ∞

Sample	Si/Al (gel)	Si/Al (sample)
A	10	12
B	18	19
C	25	27
D	50	52
E	∞	∞

catalytic applications, it will be very interesting not only to obtain ITQ-30 as pure phase, but also to synthesize the Ge-free polymorph. Then, because the results of our Pareto analysis showed that ITQ-30 zeolite is favoured with respect to ITQ-21 at low Ge content, a three-dimensional chart was generated (Fig. 5) showing that fully crystalline ITQ-30 can be obtained with the lowest Ge content studied from the more concentrated gels. Taking this into account, a new set of experiments was designed to produce a Ge-free sample. From the synthesis conditions for this set of experiments, given in Table 2, it can be seen there that Ge-free ITQ-30 can be synthesized from a Si/Al ratio of at least 10 to ∞ (Fig. 6). Chemical analyses of samples with different Si/Al ratios are given in Table 3.

The XRD pattern of ITQ-30 demonstrates that this is probably a disordered structure. However, by analogy and comparison with other XRD patterns reported in the literature, it is clear that ITQ-30 is a new zeolite with a structure that should be closely related to that of the MWW [15,16] family materials, such as MCM-22 [17], MCM-49 [18], and MCM-56 [19] (Fig. 2). The structure of MCM-22 (MWW) is very interesting, consisting of a layered precursor that forms the characteristic three-dimensional zeolite framework when calcined. It has two independent channel systems accessible through 10-ring pores, one formed by two-dimensional sinusoidal channels and the other by large supercages [16]. Related materials are the aluminosilicates PSH-3 [20] and SSZ-25 [21], the boron-containing analogue ERB-1 [22], and the pure silica polymorph ITQ-1 [23]. When the layered precursor is expanded and delayered, it produces a material with very high surface area designated as ITQ-2 [24]. The differences between MCM-22, MCM-49, and MCM-56 are mainly related to packing degree; MCM-49 presents the same framework topology as calcined MCM-22, and MCM-56 maintains its layered structure on calcination.

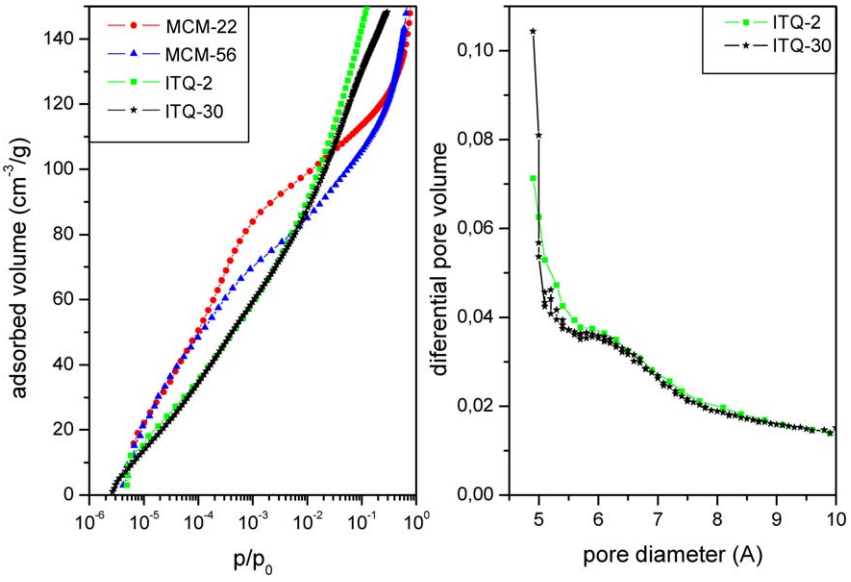

Fig. 7. Ar adsorption on different zeolites of the MWW family.

The XRD pattern of the as-made ITQ-30 zeolite (Fig. 2) shows some similarities to MCM-22, ITQ-1, and MCM-56, although the peak widths change according to the disorder. However, in the small-angle region, the differences among these materials are obvious, demonstrating that they are indeed different materials. The peaks corresponding to [001], [002], and [100] reflections are clearly visible in MCM-22, ITQ-1, and ITQ-30, but not in MCM-56. However, [101] and [102] reflections, which are separated in MCM-22 and ITQ-1, appear as a broad band in MCM-56 and ITQ-30. In MCM-56, this band has been assigned to a weighted average of one-and two-unit cell-thick crystals [25]. ITQ-30 also shows this broad reflection, suggesting that ITQ-30 is also formed by crystals of only a few unit cells thickness. However, the XRD pattern of ITQ-30 presents the bands assigned to [001] and [002] reflections in the MCM-22 precursor, which are not present in MCM-56. This indicates more order along the c direction in ITQ-30 than in MCM-56. Although we cannot elucidate the exact structure of ITQ-30, we can conclude that it is a new member of the MWW family.

To further elaborate on the structure and textural characteristics of ITQ-30, we carried out Ar adsorption. Fig. 7a compares the Ar adsorption isotherms of calcined MCM-22, MCM-56, ITQ-2, and ITQ-30. Two inflection points, assigned to the filling of 10R and 12R pores [26], are clearly observed in MCM-22 and MCM-56, whereas only the first inflection point, corresponding to the 10MR pores, is observed in ITQ-2. Surprisingly, the ITQ-30 isotherm is nearly coincident with the ITQ-2 isotherm at low pressure, and the two materials have a similar pore distribution (Fig. 7b). This could be interpreted in ITQ-30 by assuming that the 12-ring cavities are not well formed and already exhibit some "delamination." Table 4 compares textural properties of ITQ-30, MCM-22, MCM-56 [25], and ITQ-2. Although MCM-22, MCM-56, and ITQ-30 have comparable BET surface area values (much lower than the value for ITQ-2), there are some differences in the external area of these materials. MCM-22 has the lowest value, because it corresponds to a fully connected three-dimensional zeolite framework, whereas MCM-56 and ITQ-30 have similar external surface areas (although slightly higher for MCM-56), both higher than that of MCM-22.

Table 4
Textural properties of MCM-22, MCM-56, ITQ-2 and ITQ-30 samples

Zeolite	BET area (m^2/g)	Micropore area (m^2/g)	External area (m^2/g)
MCM-22	410	340	70
MCM-56	400	290	110
ITQ-2	825	115	710
ITQ-30	410	310	100

As in all MWW family members, the ITQ-30 crystals are sheets, as shown in Fig. 8. The as-made ITQ-30 samples contain 24–25 wt% of occluded organic matter, and the C/N ratio (7.9–8.1) obtained from chemical analysis indicates that the SDA is intact inside the pores with 5.0–5.5 SDA/u.c. The amount of organic is too large to be in the interlayer region, unless the "shift" of the layers suggested by Ar measurements allow incorporation of an extra amount of organic in the interlayer region. A second possibility could be that some of the SDA cations are located in the 10R channels. If this were true, and owing to the size of the sinusoidal 10R channels, then a large number of defects must be present to generate sufficient space to accommodate the SDA inside the medium-size pores. At present, we have no definitive explanation for these experimental findings.

3.1. Catalytic activity

Like MCM-56, ITQ-30 has a high external surface area, indicating the presence of a numerous external "cups" in which

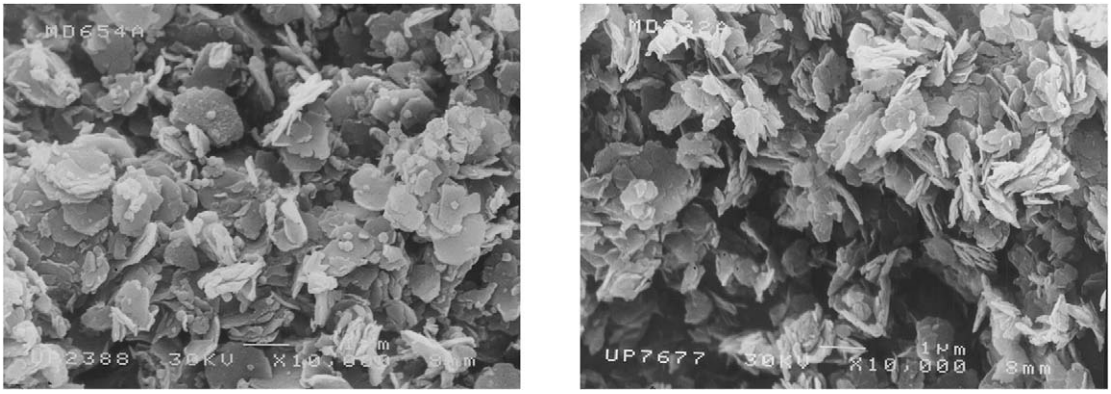

Fig. 8. SEM images of ITQ-30.

Table 5
Alkylation of benzene with propylene using different zeolites of the MWW family[a]

Catalyst	Si/Al[b] ratio	TOS = 1 h				TOS = 2 h				TOS = 5 h			
		X	S_{cumene}	S_{nPB}	S_{DIPB}	X	S_{cumene}	S_{nPB}	S_{DIPB}	X	S_{cumene}	S_{nPB}	S_{DIPB}
ITQ-30	12	99	90	0.01	9	99	90	0.01	9	98	88	0.01	10
MCM-22	15	99	88	0.02	11	99	87	0.02	12	99	85	0.01	14
MCM-56	12	99	90	0.01	9	99	90	0.01	9	99	91	0.01	8

[a] Reaction conditions: $T = 150\,^{\circ}C$, $P = 3.5$ MPa, benzene/propylene = 3.5 mol mol^{-1}, WHSV = 6 h^{-1}.
[b] Determined by chemical analysis.

the alkylation of benzene by olefins can selectively occur [27–31]. Consequently, we investigated the activity and selectivity of these materials, together with MCM-22, for the alkylation of benzene with propylene. The results, given in Table 5, demonstrate that ITQ-30 is very active for cumene production, with low selectivity to the highly undesirable *n*-propylbenzene. Note that for the results to be meaningful from an industrial standpoint, selectivities need to be given at high levels of conversion.

The results in Table 5 show that ITQ-30 and MCM-56 give very similar selectivities, in good agreement with the similar external surface area of both materials. In contrast, MCM-22 is a less selective catalyst, giving higher selectivity to n-propylbenzene, likely due to its smaller external surface area and fewer external "cups."

4. Conclusion

A new zeolite, ITQ-30, has been obtained using HT techniques applied to zeolite synthesis, together with a versatile structure-directing agent. This new material has a crystalline structure related to the MWW family and has been synthesized in a very wide range of compositions, including the pure silica and high-aluminum content aluminosilicate polymorphs. ITQ-30 is an active and selective catalyst for alkylation of aromatics with propylene. It produces very low yields of the undesired and problematic (from a processing standpoint) *n*-propylbenzene. Its catalytic behaviour is closer to that of MCM-56, as a consequence of the similar topology and external surface area.

Acknowledgment

The authors thank CICYT (MAT 2003-07945-C02-01) for financial support.

References

[1] A.W. Burton, S.I. Zones, S. Elomari, Curr. Opin. Colloid Interface Sci. 10 (2005) 211.
[2] D.E. Akporiaye, I.M. Dahl, A. Karlsson, R. Wendelbo, Angew. Chem. Int. Ed. 37 (1998) 609.
[3] J.M. Newsam, T. Bein, J. Klein, W.F. Maier, W. Stichert, Microporous Mesoporous Mater. 48 (2001) 355.
[4] P.P. Pescarmona, J.T. Rops, J.C. van der Waal, J.C. Jansen, T. Maschmeyer, J. Mol. Chem. A 182–183 (2002) 319.
[5] M. Moliner, J.M. Serra, A. Corma, E. Argente, S. Valero, V. Botti, Microporous Mesoporous Mater. 78 (2005) 73.
[6] C. Klanner, D. Farrusseng, L. Baumes, M. Lengliz, C. Mirodatos, F. Schuth, Angew. Chem. Int. Ed. 43 (2004) 5347.
[7] R.F. Lobo, M.E. Davis, Microporous Mater. 3 (1994) 61.
[8] P. Wagner, M. Yoshikawa, K. Tsuji, M.E. Davis, P. Wagner, M. Lovallo, M. Taspatsis, Chem. Commun. 22 (1997) 2179.
[9] A. Corma, M.J. Diaz-Cabañas, J. Martinez-Triguero, F. Rey, J. Rius, Nature 418 (2002) 514.
[10] R. Castañeda, A. Corma, V. Fornes, F. Rey, J. Rius, J. Am. Chem. Soc. 125 (2003) 7820.
[11] A. Corma, F. Rey, J. Rius, M.J. Sabater, S. Valencia, Nature 431 (2004) 287.
[12] B. Harbuzaru, J.L. Paillaud, J. Patarin, N. Bats, Science 304 (2004) 990.
[13] A. Corma, M.J. Diaz-Cabañas, F. Rey, S. Nicolopoulus, K. Boulahya, Chem. Commun. 12 (2004) 1356.
[14] A. Corma, M.E. Davis, Chem. Phys. Chem. 5 (2004) 304.

[15] Ch. Baerlocher, W.M. Meier, D.H. Olson, Atlas of Zeolite Framework Types, http://www.iza-structure.org/databases/.
[16] M.E. Leonowicz, J.A. Lawton, S.L. Lawton, M.K. Rubin, Science 264 (1994) 1910.
[17] M.K. Rubin, P. Chu, US Patent 4 954 325 (1990), to Mobil Oil Corp.
[18] J.M. Bennett, C.D. Chang, S.L. Lawton, M.E. Leonowicz, D.N. Lissy, M.K. Rubin, US Patent 5 236 575 (1993), to Mobil Oil Corp.
[19] A.S. Fung, S.L. Lawton, W.J. Roth, US Patent 5 362 697 (1994), to Mobil Oil Corp.
[20] L. Puppe, J. Weisser US Patent 4 439 409 (1984), to Bayer AG.
[21] S.I. Zones, US Patent 4 665 110 (1987), to Chevron.
[22] R. Millini, G. Perego, W.O. Parker, G. Bellussi, L. Carluccio, Microporous Mater. 4 (1995) 221.
[23] M.A. Camblor, C. Corell, A. Corma, M.J. Diaz-Cabañas, S. Nicolopoulos, J.M. Gonzalez-Calbet, M. Vallet-Regi, Chem. Mater. 8 (1996) 2415.
[24] A. Corma, V. Fornes, S.B. Pergher, Th.L.M. Maesen, J.G. Buglass, Nature 396 (1998) 353.
[25] G.J. Gopalakrishnan, R.F. Lobo, Microporous Mesoporous Mater. 40 (2000) 9.
[26] A. Corma, U. Diaz, V. Fornes, J.M. Guil, J. Martinez-Triguero, E.J. Creyghton, J. Catal. 191 (2000) 218.
[27] C.T. Kresge, Q.N. Le, W.J. Roth, T. Thompson, US Patent 5 259 565 (1993), to Mobil Oil Corp.
[28] P. Chu, M.E. Landis, Q.N. Le, US Patent 5 334 795 (1994), to Mobil Oil Corp.
[29] J.C. Cheng, A.S. Fung, D.J. Klocke, S.L. Lawton, D.N. Lissy, W.J. Roth, C.M. Smith, D.E. Walsh, US Patent 5 453 554 (1995), to Mobil Oil Corp.
[30] C. Perego, S. Amarilli, R. Millini, G. Bellussi, G. Girotti, G. Terzoni, Microporous Mater. 6 (1996) 395.
[31] A. Corma, V. Martínez-Soria, E. Shoneveld, J. Catal. 192 (2000) 163.